10th ANKARA INTERNATIONAL AEROSPACE CONFERENCE
18-20 September 2019 - METU, Ankara TURKEY

AIAC-2019-195

Aerostructural Design Optimization of High Speed Wings for Reusable Launch Vehicles

Andrew Cusick* and Konstantinos Kontis†
University of Glasgow
Glasgow, United Kingdom

Melike Nikbay‡
Istanbul Technical University
Istanbul, Turkey

ABSTRACT

This paper discusses the high speed vehicle optimization software under ongoing development at the University of Glasgow. Implemented in MATLAB, surface inclination methods for high speed aerodynamic computation, are coupled with a simple six degree-of-freedom finite element beam model. The resulting aerostructural system is then utilized in a population based design optimization framework. Discussions of these methodologies is provided, along with an overall outline of their combination in a typical design optimization. A detailed description of the design variables employed, along with an analysis of the management methods utilized for undesirable characteristics and infeasible configurations. Finally, an aerostructural optimization is carried out, with comparison to a previous reusable launch vehicle concept. This demonstrates the capability of the optimization framework, and highlights the future work necessary to progress the research.

INTRODUCTION

Optimization is becoming evermore popular in the aerospace engineering field, with much attention placed on high-fidelity analysis methods, particularly in terms of aerodynamics. Due to the high computational cost of computational fluid dynamics (CFD), efficiency is required in the optimization algorithm, leaving gradient based methods as the only reasonable choice. These optimizers require drastically fewer function evaluations than their gradient-free counterparts, however an additional requirement is necessary for both efficiency and confidence in the final results: a close to optimal starting point. Often then, pre-existing configurations are used as a starting point, with a design space built around its parameters. As a result, the final output may exhibit an improvement over the initial design, however the likelihood of it being globally optimal for the given objective function or functions is low. This is due to the dependency of the design space on the existing configuration; ensuring that the final result does not deviate too far from the original, while also reducing the number of function evaluations.

The overall goal of this work is to produce globally optimal super-hypersonic vehicle designs for multiple objective functions, from an arbitrary starting point. Considering the limited experience of

*PhD student in Aerospace Engineering, Email: a.cusick.1@research.gla.ac.uk
†Prof. in Aerospace Engineering, Email: kostas.kontis@glasgow.ac.uk
‡Prof. in Astronautical Engineering, Email: nikbay@itu.edu.tr

successful high speed applications, and the vast discrepancies between current concepts, it is clear that much work is required in all aspects of the design and testing phases. Here, low-fidelity analysis methods are coupled with gradient-free optimization techniques for conceptual design, allowing a large design space to be implemented that is based on engineering or flight envelope limitations, rather than that of a pre-existing configuration. Due to the drastically reduced computational power required, thousands of function evaluations can be completed at relatively low cost. This allows multiple flight states to be considered, along with regions of the search space that may result in infeasible designs or those that contain undesirable characteristics, but that cannot be quantified a priori. Results from such optimizations should allow a wide variety of optimal configurations to be analyzed based on the trade-off in their objective functions, before choosing a suitable candidate or candidates to continue the design process with.

This focus of this paper is on demonstrating the correct implementation and capability of the overall framework. Firstly, the aerodynamic and structural modelling methods employed are briefly outlined, followed by a discussion of the interface between the two disciplines, including the interpolation methods required in order to transfer data between them. The optimization method utilized is introduced, and its suitability to the problem summarized. Next, the overall architecture of the framework is described, followed by an in depth discussion of the implemented design variables, as well as undesirable traits that may arise for a given set of variables, and how these are managed. Finally, results are shown for an aerostructural design optimization, in which the Orbital Sciences X-34 [Fuhrmann, Hildebrand et al., 1999] reusable launch vehicle (RLV) concept has been chosen as a benchmark. It is important to note that this configuration is not used as a starting point, nor does it direct the optimization in anyway. However, it does place reasonable limits on the design parameters and characteristics. The reason for this is to establish that the framework is capable of producing high performance results in terms of the given cost functions, in comparison that of an existing design, under constraints determined by that configuration. It is crucial that this has been demonstrated before completely arbitrary, large design space optimizations are performed.

METHODOLOGY

Aerodynamic Modelling

At the conceptual or early design phases, flexibility and speed are desirable over high-fidelity accuracy. While CFD methods are state-of-the-art in aerodynamic prediction, the time required to analyze the thousands of configurations created in a typical large design space global optimization is unreasonable. On top of this, CFD is heavily reliant on discretization with respect to convergence and therefore accuracy. Designing an algorithm that can provide sufficient discretization not only of arbitrary vehicles, but of the complex flow domain presented by high speed flows, is far beyond the scope of this work.

Low-fidelity methods can provide rapid results purely based on vehicle geometry. While their accuracy is not up to CFD standards, it is more than acceptable for initial design optimizations covering a diverse population. In terms of inviscid flow, surface inclination methods such as Modified-Newtonian [Jaslow, 1968], oblique shock-expansion [Eggers, 1955], and Tangent Wedge/Cone [Dejarnette, Cheatwood et al., 1987] were therefore chosen for this research. Viscous effects are estimated using Eckert's reference temperature method [Eckert, 1956], with options of strip theory or streamline tracing for particle tracking. Further detail on the implemented methods, along with validation data can be found in [Cusick and Kontis, 2019].

Structural Modelling

As an initial estimation of static wing elasticity, a simple wing-box definition is reduced to a beam model. In such structures, the upper and lower skins primarily carry the bending loads on the wing, with span-wise spars supporting shear loads. Defining the wing structure in this manner allows a

straightforward box model to be created, in which cross sectional properties can be determined easily. Additional stiffness is provided through stringers, distributed evenly over both upper and lower skins. As in [Bindolina, Ghiringhelli et al., 2010], stringers at the front and rear spars are cross coupled in terms of area, while inner stringer areas are defined by a single variable. Wing-box segments are separated by beam nodes, as shown in fig. 1. The average chord of each segment is thus used in the cross-section property computation, resulting in a beam model that is representative of a series of cuboid shaped wing-box segments. A portion of the structure is also assumed to lie inboard of the wing aerodynamic mesh, representing the fuselage joint. Therefore, the innermost node is assumed to be clamped, while the second is semi-flexible [Brooks, Kenway et al., 2018]. Since the physical attributes of the wing-box are computed prior to simplification, the volume of each component and thus overall weight of the wing-box can also be determined. From here, the total wing weight is estimated using an empirical method [Elham and van Tooren, 2016]. The loads produced by the wing structure are distributed uniformly along the elastic axis and applied to the element nodes by computing the work-equivalent nodal forces and moments [Chauhan and Martins, 2018].

Once the cross-section properties and weight estimations have been computed, the wing-box segments are reduced to a single span-wise beam, connected end-to-end, allowing beam element stiffness matrices to be collated globally on block diagonals. The linear system $\boldsymbol{Ku} = \boldsymbol{f}$ is then solved using Gaussian elimination, where $\boldsymbol{K}$ is the global stiffness matrix, $\boldsymbol{f}$ is the vector of forces and moments provided from the aerodynamic solver, along with weight estimations, and $\boldsymbol{u}$ is the resulting vector of structural displacements and rotations.

To ensure that the structure has not failed under the aerodynamic loads produced in a given flight state, stress distribution and failure criteria are calculated for each beam element using the equations provided by [Elham and van Tooren, 2016]. Here, both failure due to material yield and failure due to buckling are considered. To determine the maximum allowable stress that a given structure can undergo before it fails, the equations from [Elham, Rocca et al., 2013] are utilized. Assuming the entire structure is made up of a single metal alloy, its mechanical properties can be used in determining these allowables [MIL-HDBK-5G, 1994]. Upper and lower panel buckling is calculated through the stiffened panel efficiency method, presented in [Niu, 1999], in which an efficiency factor of 0.5 is adopted, assuming a realistic z-stringer joint is present in both panels. Shear buckling is also considered for the spar webs, again discussed by Niu. A constant safety factor of 1.5 is applied to the maximum stresses, and if any beam element does not meet the failure criteria at any point in the analysis, it is assumed to be an infeasible design.

Interface

Coupling the aerodynamic and structural solvers is achieved through the use of Gauss-Seidel fixed-point iterations. This method allows each solver to run in sequence, using the data gathered from the previous output of the other, until there are no further changes in their respective outputs. This process is completed as follows: The aerodynamic module is run initially, and once forces on individual panels have been computed, they will be transferred to the structural solver, where equivalent loads on the beam nodes are calculated. Combining these forces and moments with those derived from the estimated wing weight then allows the resulting beam displacements and rotations to be found. The structural mesh motion is translated to the aerodynamic mesh, where the process is repeated until it converges. With low-fidelity aerodynamic methods being employed, the aerostructural solution can be considered to have converged once the aerodynamic mesh motion Δw, that is the change in mesh from the previous iteration, becomes negligible. In this work, we assume convergence when $||\Delta w|| < 10^{-6}$.

As arbitrary wing shapes and structures will be created and analyzed in a large design space, pop-

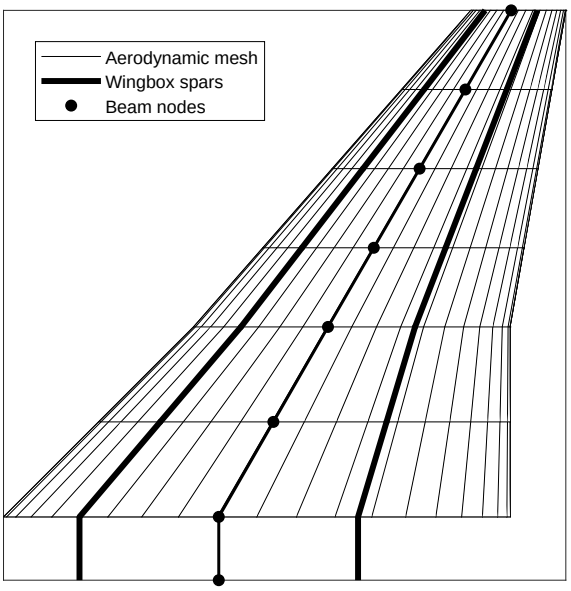

Figure 1: Aerodynamic and structural definitions

ulation based optimization, with many infeasible designs expected in the early stages, an efficient interface is required between the two disciplines. Therefore, the process is accelerated with a version of Aitken's relaxation parameter, ω [Irons and Tuck, 1969], which is applied to the structural solver. This method has been used extensively in fluid-structure interaction applications [Küttler and Wall, 2008; Kennedy and Martins, 2010; Jasa, Hwang et al., 2018]. Calculation of the parameter is done using structural displacements from previous and current iterations to accelerate the systems convergence. Once found, it relaxes the structural displacements of the current iteration, and thus the motion of the aerodynamic mesh. Since a previous cycle is required in order to calculated the parameter, a value of $\omega = 0.5$ is used for the initial cycle.

Interpolation Methods

By their nature, aerodynamic and structural definitions for a given wing configuration often result in meshes with no overlapping nodes, along with node patches that may lie entirely out with that of the partner mesh. Of course, the aim of an aerodynamic mesh is to capture the shape of a given body as precisely as possible, allowing the calculation of accurate surface properties. This results in a highly sensitive mesh with rigid requirements, which in terms of accuracy, is limited only by the choice of fluid solver. On the other hand, structural definitions for aerospace applications vary in literature from full finite element representations of typical skin, spar, rib configurations, to idealized beam or stick models. In either instance, a method is required to transfer information between meshes. As the location of aerodynamic nodes, where external forces are computed, differ from that of structural nodes, where displacements and rotations are calculated, loads and mesh motion from the respective mesh must be translated to the other.

Various methods have been utilized to achieve this. The importance however lies in a given schemes ability to transfer this information in a consistent and conservative manner, as first laid out in [Brown, 1997]. Consistency requires that the sum of forces acting on the fluid model equals that of the nodal forces applied to the structure through the principle of virtual work. In a similar manner, conservative demands that the work done on the aerodynamic mesh from displacements computed on the structural model, be equal to the work performed on the structure.

For cases where structural and fluid meshes share the same or similar boundaries, but inner nodal locations and/or mesh densities vary, bi-linear interpolation can provide a simple yet accurate transfer of information. In situations where the finite element grid is rather irregular, an area coordinate approach can be adopted. Here the FEM mesh is mapped to an unstructured triangular grid. CFD points encapsulated within the sub-triangles made from an element of the unstructured mesh are then identified, with the force being calculated from the area of these sub-triangles. Full details of this method can be found in [Guruswamy, 2002]. It should be noted that in both instances, conservation is not guaranteed, and fine grids for both disciplines are required to generate accurate results.

Linear and higher-order isoparametric finite elements such as plates or shells are often used in wing modelling, employing shape functions to transfer the local or computational space displacements to the physical domain, where they can be interpolated to the fluid grid. However, finding the location of the fluid grid points that lie within a given element in local coordinates is a more difficult challenge that cannot be performed analytically, and requires the numerical approach of inverse isoparametric mapping (IIM) [Murti and Valliappan, 1986]. Upon completion, the forces acting on the fluid nodes can be proportionally distributed to the structural element nodes. In the case of fluid nodes being out with the structural boundary, linear extrapolation must be performed. Examples of successful IIM implementation in fluid-structure interaction problems can be found in [Byun and Guruswamy, 1996; Samareh, 2007].

When fluid and structural meshes have considerably different boundaries, or perhaps the structural model lies completely within the fluid mesh, such as beam or wing-box models, the rigid link method introduced in [Brown, 1997] has proved popular. Initially introduced for CFD modelling, various high-fidelity aero-structural optimization have utilized this simple method [Martins, Alonso et al., 2005; Brooks, Kenway et al., 2018]. Coupling the two domains is achieved by finding the nearest structural node to a given node on the fluid surface, and using the vector connecting these two points to transfer information. In terms of structural displacements and rotations, this is done as follows:

$$\boldsymbol{u_A} = \boldsymbol{u_S} + \boldsymbol{\theta_S} \times \boldsymbol{r} \tag{1}$$

Where $\boldsymbol{u_S}$ and $\boldsymbol{\theta_S}$ are the displacements and rotations of the donating structural node, $\boldsymbol{r}$ is the vector defined from the structural node to the fluid node, and $\boldsymbol{u_A}$ is the resulting displacement of the aerodynamic node. Similarly, the rigid link vector is used in the translation of forces and moments from the fluid grid to the structural load vector through virtual work. It is important that the rigidity of this vector is emphasised, meaning that when an iterative scheme is applied, $\boldsymbol{r}$ should only be calculated in the pre-processing phase with the undeformed meshes. Recently, this method has also been used for low-fidelity coupling [Elham and van Tooren, 2016; Jasa, Hwang et al., 2018]. Both of the referenced works use a simple idealized beam model for the wing structure, and exploit the rigid link method by aligning the beam nodes with the fluid mesh in the span-wise direction. This means that finding the closest structural node to a given fluid point can be bypassed, and allows node specific expressions to be derived for loading and mesh motion transfer [Jasa, Hwang et al., 2018].

In terms of mesh motion, radial basis function (RBF) interpolation [Broomhead and Lowe, 1988] has grown popular in recent years, due to its versatility and ease of implementation. In this method, two arbitrary point cloud meshes, structured or unstructured, can be coupled without any code alterations required. Essentially, RBF interpolation calculates how a given node or surface point will be influenced by that of every node within a structural or aerodynamic mesh. This means that mesh motion can be easily computed from one mesh to another by simple matrix manipulation. A brief overview is provided here, however in depth explanations can be found in [Beckert and Wendland, 2001; Rendall and Allen, 2008]. The problem is formulated as follows:

$$s(\mathbf{x}) = \sum_{j=1}^{N} \alpha_j \phi(||\mathbf{x} - \mathbf{x}_j||) + p(\mathbf{x}) \tag{2}$$

In this instance, $s(\mathbf{x})$ is the function evaluated at $\mathbf{x}$, j depicts the centre or node within the mesh, with N being the total number of nodes. The function ϕ represents a radial function with respect to Euclidean distance. Many options are available for this, which can be found in [Rendall and Allen, 2008]. By setting $p(\mathbf{x})$ as a linear polynomial, the interpolation does not change, regardless of translation or rotation of the mesh, meaning coupling matrices need only be defined once in the pre-processing phase. Coefficients α_j are defined by the interpolation conditions:

$$s(\mathbf{x}_j) = y_j, \ 1 \leq j \leq N \tag{3}$$

Where y is the known positions of the centres or nodes. With the inclusion of the polynomial in eq. (2), a second requirement states that:

$$\sum_{j=1}^{N} \alpha_j q(\mathbf{x}_j) = 0 \tag{4}$$

For all polynomials q equal to or lesser degree than that of p. Importantly, this ensures that the total information transfer is equal within or between meshes, making it a conservative approach.

In the present work, the rigid link method has been employed, to be used in both virtual work transfer of forces, and mesh motion. The overriding reason for this is the choice of structural model, in this case a single discretized beam. As mentioned previously, beam nodes are aligned with the aerodynamic mesh in a span-wise direction, allowing simple coupling of the two disciplines. RBF interpolation has also been implemented, for use in future work involving physical wing-box structural definitions.

Optimization Techniques

With a large design space desired, along with low-fidelity analysis techniques employed, a population based, heuristic optimization algorithm allows efficient exploration of the search space. Particle swarm optimization (PSO) has been chosen for this work, due to the design space being almost entirely continuous. The specific version of the PSO algorithm used is similar to that of OMOPSO [Sierra and Coello Coello, 2005], which includes various methods of particle mutation, selection of the global best based on the dominating characteristics of Pareto front particles, and various other methods that focus on creating a diverse set of results [Cusick and Kontis, 2019].

While the design space in this work is mostly continuous, the output cost functions for a given set of designs are not. This is due to the fact that analyzed configurations may have attributes that are physically undesirable, but that may be seen as desirable to the optimizer, and cannot be constrained or calculated prior to analysis. In such cases, an exponential based penalty function is used, which compares vehicle characteristics to predefined minimum and/or maximum values, and applies a penalty to the cost function values depending on how far out with the boundaries a violating attribute lies. This method allows the optimizer to analyze infringing configurations without seeing them as optimal, while also not disregarding them entirely. In some cases however, a set of variables may produce an infeasible design that is unable to be fully analyzed by the cost function, an example being a wing structure that fails during aerostructural analysis. Violations that cause early termination of analysis at any point in the simulation, are given cost function values equal to infinity.

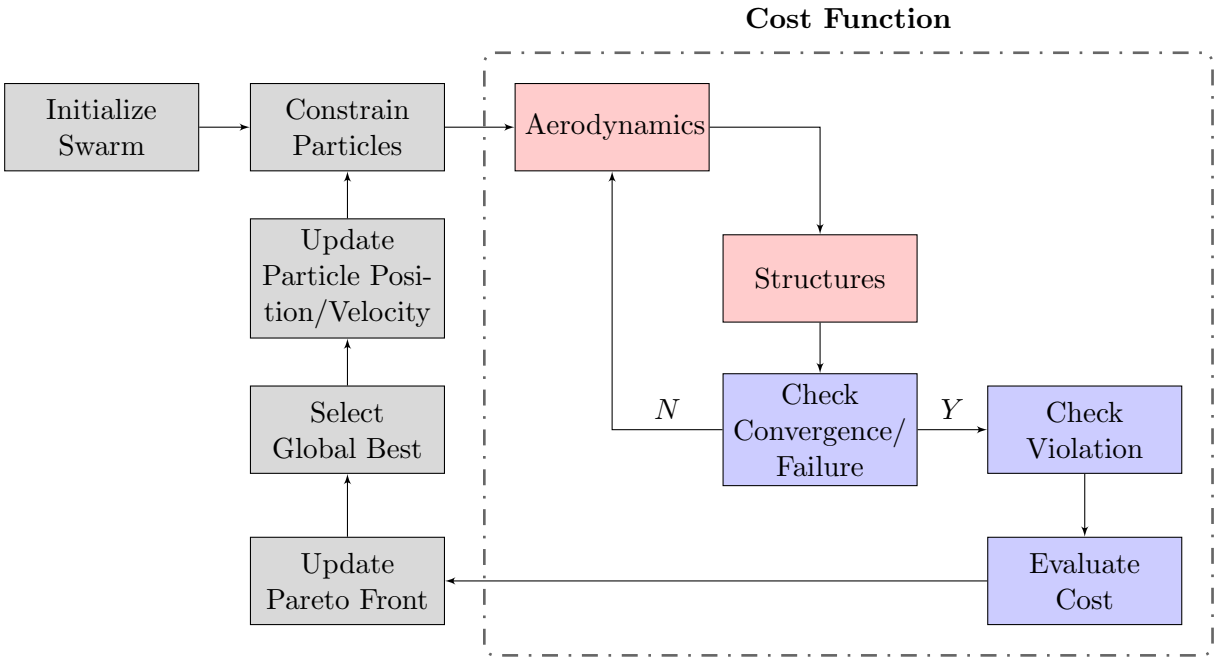

Figure 2: Multi-objective aerostructural particle swarm optimization

COMPUTATIONAL FRAMEWORK

Overall Architecture

The overall architecture of the described framework is shown in fig. 2. Particles are initialized randomly between variable boundaries. Any user-defined constraints on the design variables are applied, while also ensuring particle positions remain within the set boundaries throughout the optimization. Once constrained, the particles are passed sequentially to the objective functions, where their design variables are used to create physical configurations. The initial aerodynamic forces acting on the undeformed mesh are then computed, which are transferred to the structural solver to calculate displacements and rotations. These deformations are used to displace the aerodynamic mesh, and this process is repeated until either the convergence or failure criteria is met. If converged, overall aerodynamic and structural properties are gathered for that flight state, the aerostructural loop initializes the new flight state, and repeats until convergence is achieved for all desired flow regimes. Violation characteristics are then computed, and any penalties added to the final cost function values.

After all particle cost function values have been calculated in a given iteration, they are compared to that of the previous best cost function found by that particle, and updated accordingly. Similarly, these particle best values are compared to those of the Pareto front, with particle positions added or removed as appropriate. Global best particles are selected based their dominance of the population during the current iteration, which are used to amend particle positions and velocities for the next iteration. Finally, mutation functions are applied before particle variables are passed to the constraint manager, where the optimization loop begins again. At present, there are no widely accepted methods that define convergence of a multi-objective population based optimizer. Therefore, the PSO algorithm is run for a set number of iterations, defined by the user.

Description of Design Variables

Wing Planform:

An arbitrary number of separate wing partitions can be used to create a single wing. Each partition is defined by five parameters: dihedral, taper ratio, trailing edge sweep, span, and two-dimensional

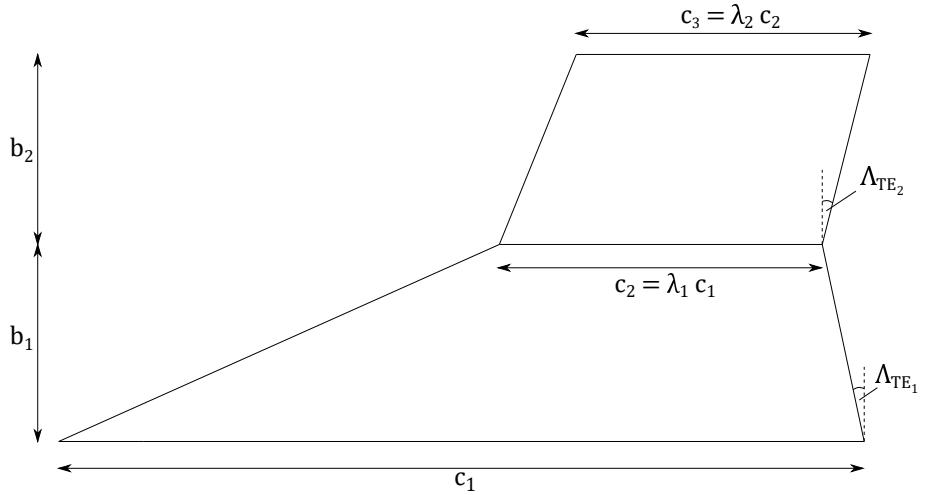

Figure 3: Planform wing design variables

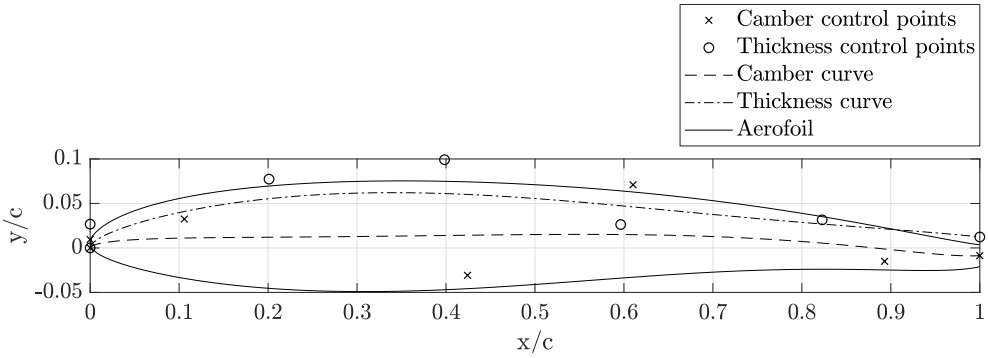

Figure 4: Aerofoil shape defined by thickness and camber Bézier curves

aerofoil section. Of course an initial root chord is required, which can be an optimization variable directly, or a ratio of fuselage length. The decision to use trailing edge sweep as a design parameter instead of defining it at the quarter chord or leading edge was to ensure that control surfaces were not made ineffective by high rearward sweep or large sweep discrepancies between partitions. Such a definition may result in undesirable sweep elsewhere on the wing chord (eg. negative sweep at the leading edge), which can be easily calculated and constrained in the analysis phase. An example of the design variables used to define a two partition wing is shown in fig. 3.

Aerofoil:

Bézier spline techniques are commonly utilized in aerodynamic shape generation, and here, two separate curves define camber and thickness of aerofoils, as shown in fig. 4. Thus, the design variables are the x and y positions of the camber and thickness curve control points. This method allows more robust control over the physical properties of the aerofoil, which will discussed later in this section. Thickness distribution is added equally in the normal directions of the two-dimension camber line, crucially providing consistent leading edge radii. It should be noted that no purely Bézier method allows for direct control over the aerofoils physical properties, since the control points affect the full curve shape, rather than acting as points for which the resulting curve must pass through.

Importantly then, a discussion is required with regards to controlling the Bézier method, to ensure that undesirable traits, perhaps clear to an engineer but not captured in an optimization or the generation method itself, do not present themselves as feasible or desirable. The Bézier method is a powerful tool that can create an infinite number of potential solutions for a given set of control point boundaries,

many of which will be unsuitable for aerofoil design. Nonetheless, particularly in a large design space optimization, it is imperative not to over constrain these boundaries, as potentially optimal solutions may be lost. In cases such as this, where optimization variables do not directly define an easily measured characteristic (such as maximum aerofoil thickness or leading edge radius), it is tempting to constrain the variables regardless, until satisfactory shapes are produced. While this may remove undesirable characteristics, it will most likely remove many feasible designs also. Instead, characteristics should be quantified once the aerofoil shape has been generated, and any undesirable traits penalized. This requires additional function evaluations on these unwanted designs. However, computational power is generally not limited in low-fidelity optimizations, making it a worthy trade-off to ensure that the broadest possible design space can be fully explored.

In turn, this raises the issue of what constitutes a large enough design space, and how can it be determined whether or not a given set of design variable boundaries is over constrained. In the present work, any method with design variables that are not themselves, or deriving from, physical properties, is first input into a purely shape optimization analysis. Here, the method is tested to ensure that it can reproduce pre-existing shapes to a specified tolerance. Assuming a diverse enough set of pre-existing designs are implemented, this approach provides a physical representation of the shape generation methods limitations, which can then easily be altered by varying the necessary optimization variable boundaries. Of course, a properly controlled method will produce feasible regardless of the variable boundaries. However, to speed up convergence of the algorithm, this trial and error approach can also be used to ensure that the design space is not unnecessarily large. In such cases, a reduction of design variable boundaries may only reduce infeasible or undesirable designs, resulting in a more efficient overall method.

For the Bézier aerofoil generation method utilized here, physical properties are calculated once the shape has been created from the two sets of control points, with penalties being applied if they do not meet user-defined requirements. Examples of such constraints will be shown in the proceeding section. This methodology allows pre-existing aerofoils to be replicated accurately, while also creating arbitrary shapes that can be easily checked for feasibility in aerospace optimization frameworks.

Wing-box:

At present, nine variables are required to create the rectangular wing-box structure introduced previously. The position of the front and rear spars are required, in terms of non-dimensional chord, as well as single values for spar and web thickness, $t_{s,w}$. The number of inner stringers has been included as a variable, N, to allow for a more versatile design space (note this is the only discrete design variable). As the stringers will be idealized as booms, three radii are required for the two sets of cross-coupled stringers at the spars, $A_{s_{1,2}}$, along with one variable that defines the radii of all those located inside the wing-box, A_{s_3}. Finally, the rib pitch is included as an optimization variable, as this is a necessary parameter in the stiffened panel efficiency method [Niu, 1999]. From these features, the wing-box cross-sectional properties can be calculated using the following equations [Bindolina, Ghiringhelli et al., 2010]:

$$A = 2 \cdot (t_s \cdot c + t_w \cdot h + A_{s_1} + A_{s_2} + N \cdot A_{s_3}) \tag{5}$$

$$I_1 = 2 \cdot \left((t_w \cdot h + A_{s_1} + A_{s_2}) \cdot \frac{c^2}{4} + \frac{c^3 \cdot t_s}{12} + A_{s_3} \cdot c_{s_3} \right) \tag{6}$$

$$I_2 = 2 \cdot \left(\frac{t_w \cdot h^3}{12} + (t_s \cdot c + A_{s_1} + A_{s_2} + N \cdot A_{s_3}) \cdot \frac{h^2}{4} \right) \tag{7}$$

$$J = 2 \cdot \left(\frac{c^2 \cdot h^2 \cdot t_w \cdot t_s}{c \cdot t_w + h \cdot t_s} \right) \tag{8}$$

Where c and h are the chord and height of the wing-box, c_s is the summed squared chord-wise distance of every inner stringer from the neutral axis. Note that since the box is rectangular, all stringers will be equidistant from the neutral axis in terms of height, hence why they have been grouped together in eq. (7). Furthermore, note that ribs are not included in the wing-box properties calculation, however their weight contribution is estimated empirically [Elham, Rocca et al., 2013].

RESULTS AND DISCUSSION

Results of an aerostructural optimization across multiple flight states is shown in the form of a Pareto front in fig. 5. As mentioned previously, a baseline wing from the X-34 configuration, has been adopted to provide constraints on designs, and present a comparison for optimal results. Note that no attempt has been made to model the X-34 structure, and thus its performance is based on a rigid airframe. The flow conditions are equal to that of the Mach 2 and 3 experiments conducted in [Brauckmann, 1999], with angle of attack cases $0°$, $10°$, and $20°$ carried out for each Mach number. The simulation was run for 1000 iterations with 600 particles, across 10 cores, and took approximately 24 hours. Optimality in this instance is defined by maximizing the average $\frac{C_L}{C_D}$ across all flight states, while minimizing wing mass. Design variables boundaries are shown in table 1, while performance, geometric, and failure constraints are briefly described in table 2. These checks not only provide a comparison to the baseline configuration, but also guide the algorithm towards feasible and desirable configurations, as opposed to those which are purely mathematically optimal.

Table 1: Two partition wing design variable set used for optimization

Variable	Minimum	Maximum	Quantity	Comments
Dihedral, *deg.*	0	10	1	Constant across wingspan
Root chord, m	8	15	1	
Taper ratio	0.1	1	2	
Sweep, *deg.*	-20	20	2	Wing trailing edge sweep
Semispan, m	0.5	4	2	Length of each partition
Spar positions	[0.05 0.6]	[0.3 0.9]	2	Non-dimensional chord location
Web/Skin thickness, m	0.001	0.1	2	
Inner stringers	1	20	1	
Stringer radii, m	0.01	0.05	3	
Rib pitch, m	0.2	2	1	
x_{c_2,t_2}	0.7	0.9	6	
x_{c_3,t_3}	0.5	0.7	6	
x_{c_4,t_4}	0.3	0.5	6	
x_{c_5,t_5}	0.1	0.3	6	Non-dimensional Bézier curve control points required for each camber and thickness aerofoil curve. Any points not shown here are set at constant (0 or 1) to anchor curves
z_{c_1}	-0.03	0.03	3	
z_{c_2}	-0.1	0.1	3	
$z_{c_{3-5}}$	-0.05	0.15	9	
z_{c_6}	0	0.01	3	
z_{t_1}	0	0.03	3	
z_{t_2}	-0.05	0.1	3	
$z_{t_{3-5}}$	-0.05	0.15	9	
z_{t_6}	0.01	0.05	3	
Total			77	

Table 2: Constraints placed on designs

Constraint	Comments
$L \geq L_{base}$	Average lift force for given Mach number at least that of baseline
$0.5\ A_{base} \leq A_{wing} \leq 1.5\ A_{base}$	Ensure wing design area remains within reason
$t_{max} \leq t_{base}$	Constrain wing and trailing edge thickness
$\frac{dt}{db} \leq 0$	Wing thickness cannot increase as span increases
$b \approx b_{base}$	Wingspan within 2% of baseline
$r_{LE} \geq r_{base}$	Ensure minimum leading edge for heating requirements
$0° \leq \Lambda_{LE} \leq 80°$	Ensure leading edge sweep remains within reason
$0.15 \leq c_{t_{max}} \leq 0.5$	Non-dimensional chord location of maximum aerofoil thickness
$\left(\frac{dt}{dc}\right)_{t\,<\,t_{max}} \geq 0$	Aerofoil thickness cannot decrease up to maximum thickness
$\left(\frac{dt}{dc}\right)_{t\,>\,t_{max}} \leq 0$	Aerofoil thickness cannot increase after maximum thickness
Failure ≤ 0	Failure criteria for all skin panels & spar webs for every flight state

Three optimal configurations are extracted from the Pareto front, and are shown in fig. 6 along with the baseline shape. Furthermore, important parameters that are not easily extracted visually are displayed in table 3. Configuration b) shows a high mass design with an impressive aerodynamic efficiency. This concept employs a thin root chord section to achieve a reduced drag coefficient, but therefore requires additional stiffness in the form of spar thickness, number of inner stringers and area of outer cross coupled stringers. Configuration c) resembles a midpoint in the Pareto front, boasting a significantly reduced wing mass from that of b), with a decreased aerodynamic efficiency. In reality however, the significant reduction of mass makes this design much more attractive. Increased wing thickness increases the spar height, making the wing considerably stiffer in bending and torsion, thus allowing thinner structures to be employed. Design d) displays a minimalistic mass option, however its aerodynamic efficiency is one of only three Pareto front designs to be less than that of the baseline configuration. Unsurprisingly, a reduced root chord is present in all of these cases, along with higher thickness to chord ratio. A combination of these two factors results in reduced skin and web thickness requirements, while the latter also produces a suboptimal aerodynamic shape.

Generally speaking, tendencies towards high taper ratios and large first partitions are present among all Pareto front designs. Furthermore, only a few configurations contain more than one inner stringer, showing a preference for thicker panels rather than additional stiffening. Of course, the low-fidelity structural model may be a cause of these tendencies, since structural failure is one of the only conditions in which analysis will be terminated early. This results in the optimization algorithm search direction having a large dependency on the structural solver with respect to any other analysis module. As a result, further flexibility is desired in the wing-box design, to ensure fewer failing configurations, and a broader search space of feasible structures.

CONCLUSIONS

Presented is a design optimization framework for super-hypersonic vehicles. Aimed at the conceptual level, low-fidelity analysis methods, along with global optimization techniques have been employed. Well known surface inclination methods have been used for aerodynamic analysis, with the wing-box being reduced to a single discretized beam to approximate structural elasticity. Gauss-Seidel fixed-point iterations have been utilized to couple the aerostructural system, with Aitken relaxation used to accelerate convergence. Particle swarm has been chosen as the optimization algorithm, due to its superior handling of continuous design space problems over other gradient-free methods. The combination of these tools has produced a versatile design optimization system capable of handling a broad design space and large number of function evaluations, without significant computational cost, or need for a pre-existing or close to optimal initial design.

A detailed description of the design variables has been provided, with explanation of a penalty ap-

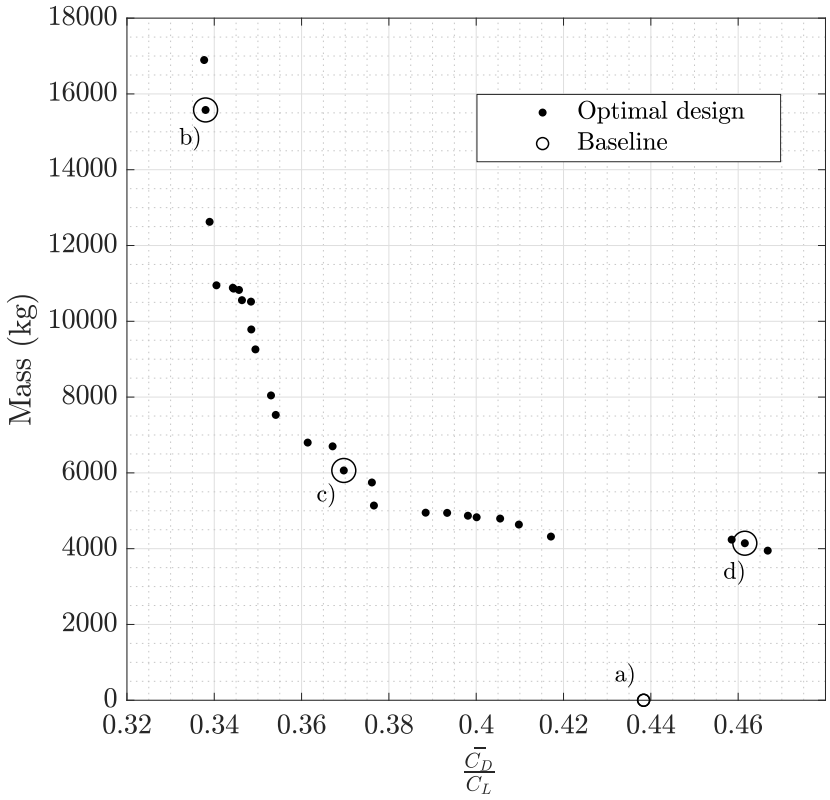

Figure 5: Aerostructural optimization Pareto front with baseline aerodynamic comparison

Table 3: Optimal design parameters

Parameters	High mass design	Trade-off design	Low mass design
A_{wing}, m^2	33.2	23.5	20.5
Dihedral, *deg.*	6.7	4.5	6.1
Spar positions	0.29, 0.61	0.3, 0.68	0.3, 0.7
Web/Skin thickness, m	0.09, 0.007	0.021, 0.002	0.017, 0.001
Inner stringers	8	1	1
Stringer radii, m	0.05, 0.04, 0.02	0.04, 0.03, 0.03	0.04, 0.03, 0.02
Rib pitch, m	1.93	1.87	1.94

proach for constraint management and undesirable characteristics. An aerostructural optimization has been performed, and select Pareto front designs compared to that of a prior reusable launch vehicle concept. Almost all optimal configurations show an improvement in aerodynamic efficiency, with further experimentation required in terms of structural solver fidelity. This will be carried out in future work, as will the implementation of a low-speed aerodynamic module, to provide a wider perspective of the flight envelope.

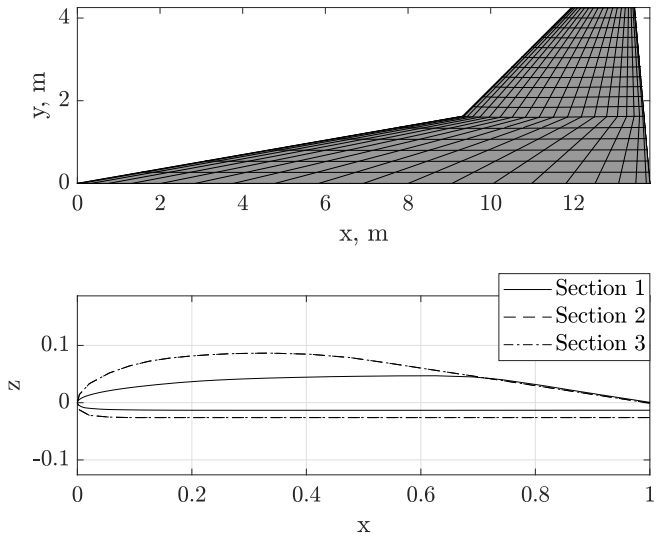

(a) Baseline

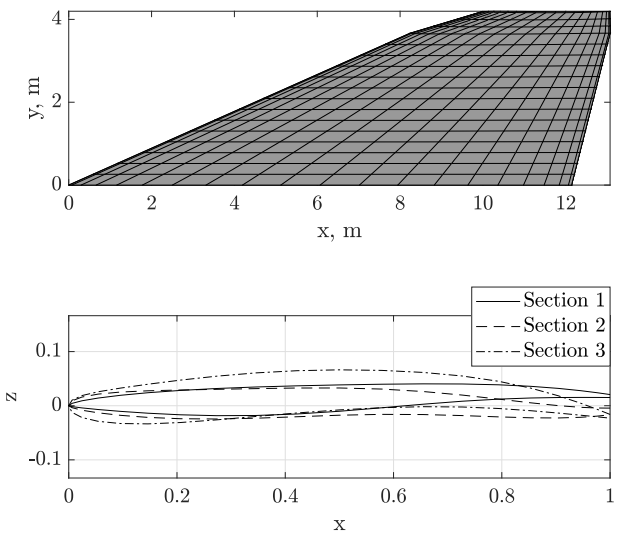

(b) High mass design

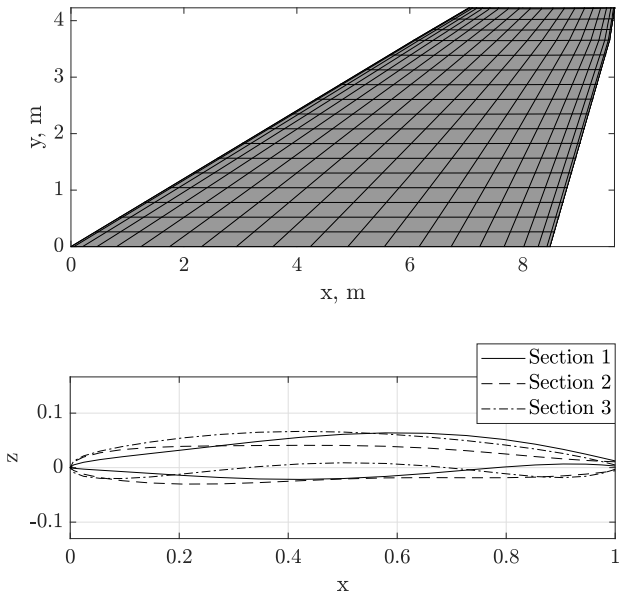

(c) Trade-off design

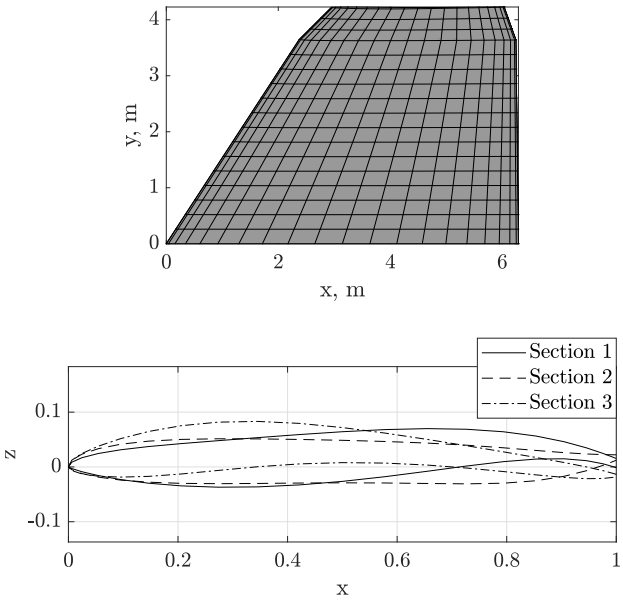

(d) Low mass design

Figure 6: Baseline and selected Pareto front configurations

References

Beckert, A. and Wendland, H. (2001) *Multivariate interpolation for fluid-structure-interaction problems using radial basis functions*, Aerospace Science and Technology, Vol 5(2), p: 125-134, Feb 2001

Bindolino, G., Ghiringhelli, G., Ricci, S. and Terraneo, M. (2010) *Multilevel Structural Optimization for Preliminary Wing-Box Weight Estimation*, Journal of Aircraft, Vol 47(2), p: 475-489, Mar 2010

Brauckmann, G. J. (1999) *X-34 Vehicle Aerodynamic Characteristics*, Journal of Spacecraft and Rockets, Vol 36(2), p: 229-239, 1999

Brooks, T. R., Kenway, G. K. W. and Martins, J. R. R. A. (2018) *Benchmark Aerostructural Models for the Study of Transonic Aircraft Wings*, AIAA Journal, Vol 56(7), p: 2840-2855, 2018

Broomhead, D. S. and Lowe, D. (1988) *Radial basis functions, multi-variable functional interpolation and adaptive networks*, Technical report, Royal Signals and Radar Establishment Malvern (United Kingdom), 1988

Brown, S. 1997 (1997) *Displacement extrapolations for CFD+CSM aeroelastic analysis*, 38th Structures, Structural Dynamics, and Materials Conference, Reno, Nevada, 1997

Byun, S. and Guruswamy, G. P. (1996) *Wing-Body Aeroelasticity on Parallel Computers*, Journal of Aircraft, Vol 33(2), p: 421-428, 1996

Chauhan, S. and Martins, J. R. R. A. (2018) *Low-fidelity aerostructural optimization of aircraft wings with a simplified wingbox model using OpenAeroStruct*, EngOpt 2018 Proceedings of the 6th International Conference on Engineering Optimization, Lisbao, p: 418-431, June 2018

Cusick, A. and Kontis, K. (2019) *Creation of Design and Analysis Tools for Large Design Space Reusable Launch Vehicle Shape Optimization*, In AIAA AVIATION Forum, Dallas, Texas, 2019

Dejarnette, F. R., Cheatwood, F. M., Hamilton and Weilmuenster, K. J. (1987) *A review of some approximate methods used in aerodynamic heating analyses*, Journal of Thermophysics and Heat Transfer, Vol 1(1), p: 5-12, Jan 1987

Eckert, E. R. G. (1956) *Engineering relations for heat transfer and friction in high-velocity laminar and turbulent boundary-layer flow over surfaces with constant pressure and temperature*, Transactions of the ASME, Vol 78(6), p: 1273-1283, 1956

Eggers, A. J. (1955) *The Generalized Shock-Expansion Method and Its Application to Bodies Traveling at High Supersonic Air Speeds*, Journal of the Aeronautical Sciences, Vol 22(4), p: 231-238, Apr 1955

Elham, A., La Rocca, G., van Tooren, M. J. L. (2013) *Development and implementation of an advanced, design-sensitive method for wing weight estimation*, Aerospace Science and Technology, Vol 29, p: 100-113, 2013

Elham, A. and van Tooren, M. J. L. (2016) *Tool for preliminary structural sizing, weight estimation, and aeroelastic optimization of lifting surfaces*, Journal of Aerospace Engineering, Vol 230(2), p: 280-295, 2016

Fuhrmann, H. D., Hildebrand, J., Lalicata, T. and Orbital Sciences Corporation (1999) *Aerothermodynamic Overview , X-34*, Journal of Spacecraft and Rockets, Vol 36(2), p: 153-159, 1999

Guruswamy, G. P. (2002) *A review of numerical fluids/structures interface methods for computations using high-fidelity equation*, Computers and Structures, Vol 80, p: 31-41, 2002

Irons, B. M. and Tuck, R. C. (1969) *A VERSION OF THE AITKEN ACCELERATOR FOR COMPUTER ITERATION*, INTERNATIONAL JOURNAL OF NUMERICAL METHODS IN ENGINEERING, Vol 1, p: 275-277, 1969

Jasa, J. P., Hwang, J. T. and Martins, J. R. R. A. (2018) *Open-source coupled aerostructural optimization using Python*, Structural and Multidisciplinary Optimization, Vol 57, p: 1815-1827, 2018

Jaslow, H. (1968) *Aerodynamic relationships inherent in Newtonian impact theory*, AIAA Journal, Vol 6(4), p: 608-612, Apr 1968

Kennedy, G. J. and Martins, J. R. R. A. (2010) *Parallel Solution Methods for Aerostructural Analysis and Design Optimization*, 13th AIAA/ISSMO Multidisciplinary Analysis Optimization Conference, Fort Worth, 2010.

Küttler, U. and Wall, W. A. (2008) *Fixed-point fluid-structure interaction solvers with dynamic relaxation*, Computational Mechanics, Vol 43, p: 61-72, 2008

Martins, J. R. R. A., Alonso, J. J. and Reuther, J. J. (2005) *A Coupled-Adjoint Sensitivity Analysis Method for High-Fidelity Aero-Structural Design*, Optimization and Engineering, Vol 6, p: 33-63, 2005

MIL-HDBK-5G *Military Handbook, Metallic Materials and Elements for Aerospace Vehicle Structures*, 1994

Murti, V. and Valliappan (1986) *Numerical inverse isoparametric mapping in remeshing and nodal quantity contouring*, Computers & Structures, Vol 22(6), p: 1011-1021, Jan 1986

Niu (1999) *Airframe Stress Analysis and Sizing*, Commit Press Ltd, Hong Kong, second edition, 1999

Rendall, T. C. S. and Allen, C. B. (2008) *Unified fluid-structure interpolation and mesh motion using radial basis functions*, International Journal for Numerical Methods in Engineering, Vol 74, p: 1519-1559, 2008

Samareh, J. A. (2007) *Discrete Data Transfer Technique for Fluid-Structure Interaction*, 18th AIAA Computational Fluid Dynamics Conference, 2007

Sierra, M. R. and Coello Coello, C. A. (2005) *Improving PSO-based Multi-Objective Optimization using Crowding, Mutation and e-Dominance*, International Conference on Evolutionary Multi-Criterion Optimization, p: 505-519, 2005